# Real-time weather forecasting in the Western Mediterranean Basin: an application of the RAMS model

(Atmospheric Research, 2014, 139: 71–89. DOI: 10.1016/j.atmosres.2014.01.011: http://www.sciencedirect.com/science/article/pii/S016980951400012X)

I. GÓMEZ[a], V. CASELLES[a,b], M. J. ESTRELA[b,c]

[a] *Departament de Física de la Terra i Termodinàmica, Facultat de Física, Universitat de València, Doctor Moliner, 50, 46100 Burjassot, Valencia, Spain.*

[b] *Laboratorio de Meteorología y Climatología, Unidad Mixta CEAM-UVEG, Charles R. Darwin, 14, 46980 Paterna, Valencia, Spain.*

[c] *Departament de Geografia, Facultat de Geografia i Història, Universitat de València, Avda. Blasco Ibáñez, 28, 46010 Valencia, Spain.*

Correspondence to: Igor Gómez Doménech

E-mail: godoi@uv.es

**ABSTRACT**

A regional forecasting system based on the Regional Atmospheric Modeling System (RAMS) is being run at the CEAM Foundation. The model is started twice daily with a forecast range of 72 hours. For the period June 2007 to August 2010 the verification of the model has been done using a series of automatic meteorological stations from the CEAM network and located within the Valencia Region (Western Mediterranean Basin). Air temperature, relative humidity and wind speed and direction of the output of the model have been compared with observations. For these variables, an operational verification has been performed by computing different statistical scores for 18 weather stations. This verification process has been carried out for each season of the year separately. As a result, it has been revealed that the model presents significant differences in the forecast of the meteorological variables analysed throughout the year. Moreover, due to the physical complexity of the area of study, the model presents different degree of accuracy between coastal and inland stations. Precipitation has also been verified by means of yes/no contingency tables as well as scatter plots. These tables have been built using 4 specific thresholds that have permitted to compute some categorical statistics. From the results found, it is shown that the precipitation forecast in the area of study is in general over-predicted, but with marked differences between the seasons of the year. Finally, dividing the available data by season of the year, has permitted us to analyse differences in the observed patterns for the magnitudes mentioned above. These results have been used to better understand the behaviour of the RAMS model within the Valencia Region.

**Keywords:** RAMS model, operational forecasting, mesoscale modelling, model verification, numerical weather prediction, natural hazards, warning and alert systems.

## 1. Introduction

The Regional Atmospheric Modeling System (RAMS) has been implemented within a real-time forecasting system over the Western Mediterranean Basin, precisely in the area delimited by the Valencia Region (Fig. 1). This area exhibits a relevant interest from a meteorological point of view, as it is particularly sensitive to certain severe weather events. Among them, we must highlight episodes of forest fires (Gómez-Tejedor et al., 1999) and heat waves (Miró et al., 2006; Gómez et al., 2010; Gómez et al., 2013) in the summer. In addition, during the late summer and autumn, episodes of torrential rains are also common over this region (Millán et al., 1995; Estrela et al., 2002; Millán et al., 2005). Finally, during the cold period of the year, the Valencia Region is affected by low temperatures, mainly related to the entrance of northerly Arctic air, entrance of north-easterly continental polar air or anticyclonic situations (Millán et al., 2005; Estrela et al., 2010).

The sensitivity of the Valencia Region to climate hazards encouraged us to design and develop a meteorological real-time forecasting system for this area (Gómez et al., 2010). Severe weather events in the Valencia Region has been studied at the CEAM (Centro de Estudios Ambientales de Mediterráneo; Mediterranean Center for Environmental Studies) Foundation, using the Regional Atmospheric Modeling System (RAMS). Besides, RAMS has also been used in the CEAM Foundation within different research projects (Gómez et al., 2010). As a result, the operational forecasting system running over the Valencia Region is based on this mesoscale meteorological model. Taking into account the climatic and physical characteristics of this region, it may be seen that the usage of an atmospheric model operating at a high resolution would be useful as a warning and alert forecasting tool and to simulate the significant local circulations and processes that take place over this region. For the current study, RAMS has been operationally implemented for the whole Valencia Region (Fig. 1) at a 3 x 3 km grid horizontal resolution. Besides, the model has been running on a daily basis for the period June 2007 to August 2010.

The attention of the current work is mainly focused on the analysis and evaluation of the RAMS high-resolution weather forecasts produced by the operational forecasting system implemented for the Valencia Region. To do this, we have taken advantage of the automatic weather stations from the CEAM network, and located within this area (Corell-Custardoy et al., 2010). Near-surface meteorological observations are compared with the RAMS forecasts in an operational evaluation. Instead of performing a verification of the model for the whole year, the evaluation procedure has been performed by dividing the available information by season of the year. This separation of the data would permit to identify the occurrence and permanence of meteorological processes typical of a concrete season of the year. Besides, this information is truly useful in order to assess the model ability to predict the corresponding atmospheric condition. On the other hand, coastal stations have been isolated from inland ones, to evaluate differences between station location, as was already done by Gómez et al. (2013).

The paper is structured as follows. Firstly, section 2 presents the data and the verification methodology. Secondly, section 3 includes the results. And finally, section 4 is devoted to the conclusions of this work.

## 2. Data and verification methodology

### 2.1. RAMS model

In this study, the RAMS model in its version 4.4 has been used. The following two-way interactive nesting domains (Fig. 1) is adopted. Firstly, Grid 1 covers the southern part of Europe at a 48-km horizontal grid resolution and the Mediterranean. Secondly, Grid 2 covers the Iberian Peninsula and the western Mediterranean with a grid resolution of 12 km. Finally, a high resolution domain (3 km) (Grid 3) includes the Valencia Region. In the vertical, a 24-level stretched scheme has been selected, with a 50-m spacing near the surface increasing gradually up to 1000 m near the model top at 11 000 m. A summary of the horizontal and vertical grid parameters is provided in Table 1. Although the number of vertical levels does not permit a so high model top, this grid configuration has been selected looking for a compromise between the model being able to simulate the most significant local circulations over this region in a time where the forecast is useful and the computational resources available when the model was implemented that way. Nevertheless, as only surface variables are analysed in the current work, we strongly believe that the model top employed is adequate to fulfill the purpose of this study. Furthermore, we must remark that, in terms of temperature and wind speed and direction, the results found in the present study are comparable to those found in other studies using additional vertical levels and reaching a higher model top (Palau et al., 2005; Pérez-Landa et al., 2007).

The RAMS model includes different options for parameterizing physical processes (Pielke, 2002; Cotton et al., 2003). In the present study, the Mellor and Yamada (1982) level 2.5 turbulence parameterization is used. Besides, a full-column two-stream single-band radiation scheme that accounts for clouds to calculate short-wave and long-wave radiation (Chen and Cotton, 1983), and the cloud and precipitation microphysics scheme from Walko et al. (1995) is applied in all the domains. The Kuo-modified parameterization of sub-grid scale convection processes is used in the coarse domain (Molinari, 1985), whereas grids 2 and 3 utilizes explicit convection only. This convective scheme has been adopted based on previous studies performed within the area of study (Palau et al., 2005; Pérez-Landa et al., 2007). Finally, the LEAF-2 soil-vegetation surface scheme was used to calculate sensible and latent heat fluxes exchanged with the atmosphere, using prognostic equations for soil moisture and temperature (Walko et al., 2000).

RAMS initial and boundary conditions are derived from the operational global model of the National Centre for Environmental Prediction (NCEP) Global Forecasting System (GFS), at 6 h intervals and 1 x 1 degree resolution globally, using a Four-Dimensional Data Assimilation (FDDA) technique applied to define the forcing at the lateral boundaries of the outermost five grid cells of the largest domain. Weather forecasts were performed twice a day, at 0000 and 1200 UTC using the GFS forecast grid from its forecast cycle 12-h earlier, and for a forecast range of three complete days (today, tomorrow and the day after tomorrow). However, only the information corresponding to the 0000 UTC RAMS forecast was stored as will be described later. Finally, RAMS forecast outputs are available once per hour for display and analysis purposes. Thus, the model verification has been limited in time to a frequency of 1-h, regardless of the frequency of available observational data.

**2.2. Observational data**

The CEAM automatic surface weather stations network provides a good coverage of observations within the Valencia Region (Corell-Custardoy et al., 2010). However, some of this meteorological stations are located in peaks at a high altitude for use in the research of passive fog collection (Estrela et al., 2008), that the model is not able to reproduce using the current configuration. Thus, we have selected those stations in which the model is able to properly reproduce not only the orographic and physical conditions of the station location but also its surroundings. In this sense, only those stations with a difference in altitude between the station and the corresponding grid point lower than 50 m have been selected to carry out the verification of the model. This threshold in altitude has been chosen as it is approximately the thickness of the first model level using the current configuration. Due to the low density of pure coastal stations, we have merged them with pre-coastal ones. However, the behaviour of the model for those sort of stations, although nearer the one observed for the coast, is in between this locations and those placed inland, depending on the station location (not shown). As a result, a total of 6 coastal stations (including pre-coastal ones) and 12 inland stations has been selected (Fig. 1).

Although the CEAM weather stations network stores data in a 10-minute basis, hourly measures of air temperature, relative humidity, wind speed and direction and precipitation from this network have been used in the verification process, in order to match the RAMS output frequency.

**2.3. Verification procedure**

RAMS output from the higher resolution domain are compared with the observations. We have developed a software tool to extract and store, for each daily simulation within the period June 2007 to August 2010, the hourly RAMS forecast temperature, relative humidity, wind speed and direction as well as precipitation at each selected CEAM station location using Grid 3 (Fig. 1). These data have been stored for the three days of simulation of the model. More information about the software developed may be found in Gómez et al. (2013).

Several processes are carried out in the RAMS evaluation. A series of statistical scores have been computed for each CEAM station independently (Papanastasiou, 2010; Federico, 2011; Kotroni, 2011; Hernández-Ceballos et al., 2013). The statistical calculations carried out in both cases include the mean bias, root mean square error (RMSE) and the index of agreement (IoA) for the near-surface temperature, relative humidity and wind speed. Additionally, the RMSE for the vector wind difference (RMSE-VWD) is computed as well. Firstly, bias (or mean bias) is defined as the average of the simulated value minus the observed value and quantifies the systematic error of the model. Secondly, RMSE is the square root of the individual differences between simulated and observed values; it quantifies the accuracy of the model. In this sense, the RMSE-VWD corresponds to the RMSE of the horizontal vector-wind-difference. In the third place, the IoA is a modified correlation coefficient that measures the degree to which a model's prediction is free of error. A value of 0 means complete disagreement while a value of 1 implies a perfect agreement. Finally, besides computing the mentioned statistical scores, the observed averaged value and modelled averaged value are computed as well for graphical depiction purposes.

In the case of precipitation, and as a difference with the results observed for other meteorological variables, no specific pattern has been found among coastal and inland stations. Thus, to introduce the results for this magnitude, all stations has been merged (Fig. 1). The verification of precipitation, includes the forecast of the total daily accumulated precipitation amount, starting at 0000 UTC, as well as the four 6-hourly accumulated precipitation forecasts of the day. With this data, a 2x2 contingency table (Martin et al., 2010) is then constructed for some precipitation thresholds. The values selected are those used by Bartzokas et al. (2010), 2, 8, 15 and 30 mm. With the contingency tables generated, categorical statistical scores are computed in order to describe particular aspects of precipitation forecast performance (Mazarakis et al., 2009). The categorical statistics include the accuracy (AC), bias score (BIAS), probability of detection (POD), false alarm ratio (FAR), threat score (CSI) and the Heidke skill score (HSS). AC expresses the fraction of the correct forecasts. That is, the percentage of observed yes events in addition to correct negatives that were properly forecast. BIAS measures the ratio of the frequency of forecast events to the frequency of observed events and it indicates whether the forecast system has a tendency to under-predict (BIAS<1) or over-predict (BIAS>1) events. POD expresses the fraction of the observed yes events that were correctly forecast. FAR expresses the fraction of the predicted yes events that actually did not occur. CSI measures the fraction of observed and/or forecast events that were correctly predicted. As a result, CSI is only concerned with those forecasts where correct negatives are not considered. Finally, HSS measures the fraction of correct forecasts after eliminating those which would be correct due purely to random chance (Bartzokas et al., 2010).

Concerning precipitation, it is well known that the standard categorical verification statistics computed from point match-ups may lead to poorer verification results, specially regarding the double penalty problem (Rossa et al., 2008). Therefore, spatial verification methods may be desirable if the measurement data is accessible on a grid, as the analysis of the model data depends on its horizontal resolution. However, the available data in the current study is that corresponding to the rain gauge network (Fig. 1). Thus, the approach applied will be focused on the traditional metrics described above. Nevertheless, it is important to highlight that the purpose of this verification process is to evaluate the RAMS model precipitation for each season of the year separately. In this regard, the model configuration and the rain gauge available information is maintained throughout the whole verification period. As a consequence, we strongly believe that the procedure used in the present work is still helpful and appropriate to obtain a global evaluation of the RAMS-simulated precipitation and to remark the characteristics of rainfall forecasts for the different seasons of the year in the Valencia Region.

The operational verification for all the meteorological variables has been carried out for all days of simulation independently: today, tomorrow and the day after tomorrow, and all seasons of the year separately. Dividing the information for each day of simulation will permit to evaluate the degree of the forecasts as the simulation progresses and define the skill of the model that will be expected from its initialization. Dividing the available data for each season would permit to evaluate the skill of the model in reproducing the meteorological characteristics within the Valencia Region for each season. Winter is defined by the months December-February, spring for months March-May, summer from June to August and the fall within the period September-November. From the period of verification, a total of 3 winters (2007-2008, 2008-2009, 2009-2010), springs (2008, 2009 and 2010) and falls (2007, 2008 and 2009), and 4 summers (2007, 2008, 2009 and 2010) have been used in this study. For each of those periods, the statistical scores for temperature, relative humidity, and wind speed and direction, has been computed for each station individually. It has been found that all coastal stations present similar results for a particular season of the year, and the same is also true for inland stations. However, the behaviour of the model in forecasting the evaluated magnitudes for coastal stations is rather different for that found for inland ones. Thus, taking this results into account and in order to clarify the presentation of the results, the different stations have been divided by areas: coastal and inland stations. All data for each sort of stations and for each season in each available year has been merged and a series of statistical scores have been computed again as well as merging all stations for each season. To make the paper clearer, we present here the differences between coastal and inland stations in a seasonal way taking into account all data available for all years. The behaviour of the model found for maximum and minimum temperature taking into account coastal and inland stations separately is in accordance with the results found over this area by Gómez et al. (2013).

## 3. Results

### 3.1. Temperature and Relative Humidity

The average hourly evolution of the near-surface temperature and relative humidity is included in Fig. 2c,d for the summer season. It is seen that, in the early morning until noon, the near-surface temperature is very well captured by RAMS. On the contrary, from this time on and at night, the model shows slightly higher temperatures compared to the observations. The differences between the temperatures observed and forecast are related to a greater deviation in the near-surface relative humidity. In this sense, higher disagreement in relative humidity between the observations and the model is found within this period of the day for both inland and coastal stations. In the first sort of stations, a significant difference in relative humidity has been found between day and night time. During the day time, the variance between the modelled relative humidity and the observed one is quite reduced, and the model is able to capture quite well the maximum temperature. In contrast, during night time, this difference in relative humidity raises significantly, with an overestimation of the minimum temperature. For coastal stations, it is also shown that the model is able to simulate the relative humidity observed around sunrise, with the temperatures very well captured for this period. Besides, the differences found between the modelled and observed relative humidity for the rest of the day are rather alike. Thus, as it was already stated by Gómez et al. (2013), during summer a different behaviour of the temperature is observed between day time hours and night time for both coastal and inland stations in the Valencia Region.

Within this season of the year (Table 2), the IoA of the temperature for all stations is around 0.9 for coastal stations and inland stations during day time, indicating that the evolution of this magnitude is very well reproduced by the model. In general, RAMS reproduces a slight overestimation of temperature, with a global bias of 1.0 ºC for the first day of simulation. It can be seen how the tendency of the model is the same for day and night time. When only the coastal stations are considered, the model has a very little bias (0.4 ºC) for the whole day. For inland stations, the model has a global positive bias of 2 ºC. At night, more differences are observed. In this case, the tendency of the model is the same as the one observed during the day, producing a positive bias of 3 ºC, compared to a bias of 0.4 ºC for the day. Nevertheless, a high value of 0.7 for the IoA score at night is still observed. These trends are also observed in Fig. 3c,d. In relation to the relative humidity, RAMS simulates this magnitude worse than it does for temperature (Fig. 4c,d). The IoA for the relative humidity is lower than that computed for temperatures, with values between 0.5 and 0.7 approximately. The IoA is greater for both sort of stations during day time. It is greater than 0.7 for inland stations, i. e., reproducing quite well the day-to-day evolution of relative humidity. On the contrary, at night, this value falls to about 0.6, indicating that the model has more difficulties in capturing the evolution of this magnitude for this period of the day. The model is too dry both at night and during the day time, as it is reflected by a negative bias in all situations analysed (Figs. 2 and 4), but with different degree of accuracy for coastal and inland stations. In this sense, better results in the relative humidity forecasts are found for the night time and for coastal stations, with bias of -13 % opposite to a value of -20 % for inland ones and for the first day of simulation. At day time, a bias between -8 and -9 % is found for both sort of stations. Thus, the dry bias is more pronounced at night inland. In addition, there are low differences for the bias score between night and day in the coast. During summer time, the IoA for the relative humidity suffers a slight decrease for the second and third days of simulation in all cases, while both the bias and RMSE increase in general as the simulation progresses (not shown). Finally, the RMSE statistics for temperature is about 3 ºC, with higher values for inland stations at night, while the model shows values of RMSE around 23 % for relative humidity.

Similar results as those commented within the summer season are found in the spring, as can be seen in Table 2. However, Fig. 2a,b reflects that the difference in relative humidity both for coastal and inland locations is reduced compared to the summer.

In the winter, for inland stations, the model captures quite well the temperature evolution (Fig. 2g,h). However, the model has some difficulties in the daily heating and cooling. In contrast, the modelled and observed differences in relative humidity are quite reduced in the winter (Fig. 4g,h). As a consequence, the magnitude of the minimum temperature is better captured for this season of the year, although a delay in the time occurrence of about an hour is also observed. For coastal stations, the model has a tendency to delay the daily cooling. In this sense, it can be seen that, although the cooling observed stabilizes soon in the evening, the model continues this process. Thus, the minimum temperature is under-predicted by the model. This delay in the daily cooling produces the model to be also delayed in the daily heating. As a consequence, the forecast maximum temperatures are lower than those observed. The difference in the daily temperature evolution shows its relation to the relative humidity, where it can be seen that the significant cooling modelled by RAMS is associated with the rising curve of relative humidity while the observed magnitude is nearly constant during the end of the evening and the whole night.

Table 2 shows that the IoA for the temperature is above 0.9 during the day-time while it falls at night-time. Besides, low negative bias are found for coastal stations for the whole day. For inland stations, the model has a bias of -0.9 ºC at day-time, thus producing a slight under-prediction of the temperature observed. In contrast, the model shows a low over-prediction of the temperature at night, as shown in the bias score (0.8 ºC). For this sort of stations, values up to 4 ºC are found for the RMSE statistics.

The IoA during the fall season (Table 2) for temperature shows values greater than 0.9. Thus, the model is able to capture very well the daily and day-to-day evolution of this magnitude. Besides, low values for the temperature bias score, below 1.0 ºC, are also found in general for both sort of stations. In terms of relative humidity, the model shows a general tendency to under-predict the observations (Fig. 4e,f), but with lower differences than those found in the summer and the spring, and rather similar to those obtained for the winter season.

As shown in Fig. 4 there are significant differences in terms of relative humidity between the summer and the winter seasons when comparing the simulation with the measurements. In this sense, the summer season is characterized by a notable underestimation of this magnitude while the winter shows a tendency to overestimate the observations in general. As it will also be seen later for the wind field, the spring and the fall stay in between the other two seasons, with the spring closer to the summer results and the fall nearer the winter pattern.

### 3.2. Wind Speed and Direction

The wind regime within the summer season (Fig. 5c,d) is characterized by the development of a diurnal sea-breeze advecting air from the sea to land, and a surface drainage wind from land to sea at night. It is seen how thermal circulations develop during the day, producing this advection pattern. The sea-breeze flow stabilizes during the central period of the day, as can be seen in the nearly flat curve described both by the observation and the model output for wind direction. In this case, the model reproduces very well the observed South-Eastern flow merging all stations. Besides, the summer wind transition is more marked for coastal stations both in the observations and the model.

The IoA for the wind speed is 0.4 for the first day of simulation merging all sort of stations and during day time (Table 3), while it rises up to 0.5 at night time. In the first case, a value of 3 m/s for bias is observed, while at night, bias is lower, with values about 1.1 m/s, as it was already seen above in the time series plots. These values are fair good, due the complexity of the flow, which is more marked during the day time. For wind speed, the model is too windy both at the coast and inland, with the model performances better during the night in both cases (Fig. 6c,d). The RMSE is about 2 m/s taking into account all stations. Finally, the RMSE-VWD reflects the day-night differences for the wind speed, as was already shown in Fig. 5c,d.

During the spring season, RAMS is able to capture rather well the wind flow regime Fig. 5a,b. For coastal stations, the transition between both breeze processes is well reproduced by the model. However, wind speed for this kind of stations is overestimated by the model. For inland stations, the model is able to capture very well both the wind flow regime and the daily transitions as well as the wind speed observed. Furthermore, RAMS is able to reproduce better the wind field observed at night than it does at day time (Fig. 6a,b), as indicated by the values of the RMSE-VWD statistics.

During the fall season, there is a marked increase in drainage flow compared to the sea breeze circulation, coinciding with a reduction of sunlight hours (Fig. 5e,f), which is more pronounced for the winter (Fig. 6g,h). In this last case, for coastal stations, this diurnal wind flow regime transition is maintained, although followed by a reduction in the regime flow amplitude. In this case, this transition is very well captured by the model. For inland stations, this wind flow regime is significantly reduced. In this case, land breeze controls the wind circulation and it is maintained practically throughout the whole day (Fig. 6h). RAMS captures quite well the time evolution of this wind flow, although it provides northerly winds. Besides, the wind speed is very well captured by the model for inland stations.

In terms of the model error for the wind speed (Table 3), the model is able to capture very well this magnitude for inland stations during the winter, with low bias merging all data. However, for coastal stations, the model is slightly windy. When taking into account all data, a bias of about 0.9 m/s is obtained. Comparing the statistics for the wind speed between the winter and the summer seasons, better results are found for this statistics within the first one, specially during the day-time. Furthermore, Fig. 6 shows the significant differences that are reproduced by RAMS between the winter and the summer seasons for all sort of stations. In this sense, RAMS establishes a well separated transition between two wind flows of different characteristics in the summer: drainage wind from land to sea at night and sea-breeze during the day. In this case, as it was pointed before, the model remains too windy in the case of a sea-breeze flow compared to the observations. However, this difference is not so clear in the winter season, where the model reproduces a larger dispersion of the data (Fig. 6g,h), indicating more variability in the wind field. In the end, the spring and the fall seasons represents situations in between both cases described: the first one, close to the results found for the summer but not as notable as in this case, while the fall reproduces a similar pattern to the one found for the winter. In this case, it is still observed the transition between the summer and the winter (Fig. 6e,f).

Finally, considering the RMSE-VWD for all stations, no significant differences are found comparing the different seasons of the year. However, the fall is the period where lower values of this statistics are recorded, but close to the values observed within the other periods.

**3.3. Precipitation**

The comparison between the modelled and the observed daily accumulated precipitation for the second day of simulation is presented in Fig. 7 for all seasons of the year. This figure shows that RAMS presents a clear tendency to underestimate higher values of observed precipitation. This is the pattern reproduced by the model throughout the year, independently of the corresponding season. However, the model shows the opposite trend for low precipitation. Moreover, RAMS forecasts large values of precipitation not observed. Once again, this is the pattern followed by the model throughout the year, with the exception of the winter. Even though this trend is maintained for this season of the year, it is not as pronounced as the one reproduced within the other seasons.

When dividing the accumulated precipitation data by 6-h periods, it is observed that RAMS produces a significant overestimation of the accumulated rainfall for the first 6-h interval (00:00-06:00 UTC) within the first day of simulation (not shown). This result is not observed for other time periods. Thus, although the model shows rather similar results for the three days of simulation in the second (06:00-12:00 UTC), third (12:00-18:00 UTC) and fourth (18:00-24:00 UTC) intervals, more differences are observed for the first 6-h period, causing unrealistic results of the forecast precipitation for this whole first day of simulation. As a result, comparing the three days of simulation, it is observed that the accuracy of the model slightly decreases as the simulation moves forward. Nevertheless, it has been found that for the first day of simulation, the model skill is lower than that found the second day, due to the mentioned overestimation during the period 0-6h within the first day. This result is not related to a particular season. On the contrary, it is a constant for all seasons of the year. Besides, this result is not found for the second and third days of simulation.

During summer, the tendency of the model to over-predict the observations is more notable within the period 12-18h (Fig. 8g), where more differences are found with the other time intervals. This result apply to the other seasons of the year, as shown in Fig. 8c for the spring.

From all seasons of the year, the fall is the one where the largest values of accumulated rainfall are observed in the Valencia Region (Fig. 7). In this case, considerable precipitation is distributed along the whole day (Fig. 9). In the winter, rainfall is observed throughout the whole day, with higher amount of precipitation starting in the second 6-h interval (06:00-12:00 UTC) (Fig. 9f). Spring and summer seasons show rather alike results in terms of accumulated precipitation for the different 6-h intervals. In this case, higher amounts are observed in the third 6-h interval (12:00-18:00 UTC), specially in the summer where thunderstorms are common over the area of study. These results of precipitation observed agree with the study of Millán et al. (2005), where it was pointed out that within the Valencia Region, summer thunderstorms are associated with the final stages of development of the combined sea breeze/upslope winds, and they tend to develop on the east-facing slopes of the coastal mountain ranges from noon, as has also been shown here.

Categorical statistics of the contingency tables for 2, 8, 15 and 30 mm daily precipitation thresholds has been computed for the three days of simulation and all seasons of the year (Table 4). In general, it has been found that POD, CSI and HSS decreases as the precipitation threshold increases, with the FAR score following the opposite trend. In addition, for higher thresholds the model shows more difficulties in forecasting the observed precipitation pattern. Besides, it is important to note that the rainfall prediction within the summer is poorer than in the other seasons of the year, increasing the FAR score. The model has a tendency to over-predict the observations in all seasons, as indicated by the positive values of the bias score, being more marked for higher thresholds. Comparing the three days of simulation separately, the first day presents the largest values of POD, CSI and HSS scores, with the lowest value of FAR statistic (not shown). However, the accuracy of the model over this period is lower than the one computed for the other two days of simulation. Besides, the bias score is higher within the first day of simulation, with higher differences for larger thresholds. Once again, these differences seem to be related to the total precipitation forecast by the model within the first 6 hours of the simulation, that was not observed. Comparing the different scores by season, it is seen that although the tendency of the model in the fall is the same as in the other seasons of the year, RAMS is more accurate in this case, specially for the highest thresholds. In addition, the model is skilful in reproducing the forecast of precipitation properly at a percentage better than 90 % in general, as indicated by the AC score. Taking into account a particular threshold, there are no significant differences between the four seasons of the year. The largest deviation between seasons is located in the bias score, specifically for the maximum thresholds selected. In this case, the rainfall observed is better represented by RAMS in the fall and the winter. In contrast, the spring and the summer show the largest differences between the observations and the model.

The above verification process has also been followed using the four 6-h periods of the day. In tables 5-8 the results for the daily 6-h period of the second day of simulation are presented. As in Bartzokas et al. (2010), the 30 mm threshold has been omitted because of the too low number of events. In addition, as may be observed in the mentioned tables, the 15 mm threshold cannot be considered decidedly convincing for the same reason. For the period 00:00-06:00 UTC, there is a clear trend of the POD, CSI and HSS scores to decrease as the threshold increases in the spring, summer and fall. On the contrary, FAR increases for higher thresholds. During winter, however, this trend is not so clear. Moreover, within this season, the bias increases for higher thresholds, as a difference with the other seasons of the year.

A relevant result that has been mentioned in this section is that the model presents difficulties in forecasting the observed precipitation for the first day of simulation (not shown). Thus, larger values of bias are found within the period 00:00-06:00 UTC compared to those found for the second and third days of simulation. As a result, the greatest errors found for the first day of simulation within the 24 hours are related to this significant overestimation of precipitation within the 00:00-06:00 UTC period of this day. These differences are found for all seasons of the year, being more notable during the summer and the spring. Besides, tables 7 and 8 show that for these seasons of the year, higher values of bias are produced by RAMS within the period 12:00-18:00 UTC for the highest thresholds, as well as within 18:00-24:00 UTC. As introduced above, in the summer season, episodes of thunderstorms are frequent over the Valencia Region (Millán et al., 2005). Thus, the model is in general overestimating the amount of precipitation recorded in these sort of events. As a result, the overestimation observed in the summer and the spring for the 24-h accumulated precipitation is related to the high differences in the period 12:00-18:00 UTC for all days of simulation. In addition, for the first day of simulation, these differences are reinforced with those found within the period 00:00-06:00 UTC. This could be related to the initialization of the model. In addition, a recent study carried out by Gómez et al. (2011) shows the influence and the impact of convective parameterization in the RAMS model results for a heavy rain event within the Valencia Region. As a result, it seems that the effect of the convective parameterization configuration used in this operational forecasting system should be considered in the future in order to improve the precipitation forecasts over the region of study.

## 4. Conclusions

The RAMS model has been running operationally for the period June 2007 to August 2010 within the Valencia Region. The results are used in order to develop a meteorological high-resolution real-time forecasting system focused on the forecast of meteorological and climatological hazards. The main aim of this paper has been to perform an evaluation of the operational forecasting system implemented in the Valencia Region. In this sense, a seasonal verification has been applied dividing the surface weather stations by coastal and inland locations. Separating both sort of stations permit to evaluate differences for the model forecasts in a regional way, as well as to obtain more information of the model skill. As a result, it has been found that differences arise in all variables analysed between coastal and inland stations, except for precipitation. Moreover, the model behaves in a different way throughout the year for these stations, with marked seasonal characteristics, particularly between the summer and the winter.

The following conclusions can be drawn according to this verification analyses. Firstly, temperature is rather well captured by the model for coastal stations in the spring and the summer. However, more differences are found during the fall and the winter. The time of minimum temperature in the summer is very well reproduced by the model, but delay is found for the rest of the seasons, specially in the fall and the winter. For inland stations, day time temperature is slightly overestimated in the spring and the summer, but is properly captured in the fall and the winter. In contrast, a significant over-prediction of the night time temperature is found in the spring and the summer. This magnitude is rather well reproduced by the model in the fall and the winter seasons. In addition, the model follows correctly the diurnal heating observed in the spring and the summer, for all kind of stations. Moreover, the model captures quite well the night cooling in the fall and winter. On the contrary, the model has more problems while simulating this process in the summer.

Secondly, the relative humidity is in general under-predicted by the model for all seasons of the year, but this difference is remarkably more notable during summer, both for coastal and inland stations. Thus, the model is too dry, specially at night and in the summer, producing the model to be too warm within this period of the day. In contrast, in the fall and winter, the tendency of the model changes from day time to night time, mainly in winter and for coastal stations. For inland stations within this period of the year, the evolution and magnitude of the relative humidity is very close to one observed. In all cases, there is a period, between 8:00 and 10:00 UTC, for both spring and summer, coinciding with the wind flow transition from night time land breeze to day time sea breeze, where the model captures very well the relative humidity observed.

In the third place, surface wind direction is rather well reproduced by the model for both inland and coastal stations, accounting for the daily regimes and cycles observed. Moreover, the onset of the wind flow transition from night time land breeze to day time sea breeze is also well captured by the model. In terms of surface wind speed, this magnitude is properly simulated by RAMS both at night and day time for inland stations in all seasons. In this case, greater differences between the modelled and observed results are found in the summer season. For coastal stations, the model shows greater differences, mainly at day time and during the summer. Thus, the model is too windy, specially over coastal stations, reducing the skill of the model in forecasting this magnitude. Nevertheless, the daily and day-to-day evolution is in general fairly captured by the model.

Finally, the precipitation forecasts are in general acceptable taking into account the restrictions and limitations in the initialization of an operational forecasting system as the one described here. However, the model shows a clear tendency to overestimate the observations, as shown in the categorical statistics computed for the 24-h and the 6-h accumulated precipitation. It has been observed that this behaviour is more marked for the first day of simulation, due to a significant over-prediction of the RAMS-simulated accumulated rainfall within the first 6-h interval (00:00-06:00 UTC). This result causes unrealistic elevated amounts of simulated precipitation for this day of simulation, and seems to be the reason for the higher differences found in the 24-h accumulated rainfall for this day compared to the second and third days of simulation.

As a final conclusion of the results shown in this work, it can be said that the implementation of the RAMS model presented in this study as a forecasting tool within the Valencia Region works properly. The results found for air temperature, relative humidity, wind speed and direction, and precipitation are very similar as well for the three days of simulation, with the exception the first 6-h precipitation totals for the first day of simulation. However, some issues, as the initialization of the model, should be investigated more in depth to evaluate possible methodologies that improve the model results. Besides, the performance of the radiative transfer parameterizations used in mesoscale models have a strong impact on the meteorological variables analysed within this paper. It is well known that radiation is one of the most important physical processes that drives the thermal circulations described. Thus, this information should be taken into account. Furthermore, the same model configuration has been maintained throughout the year. However, significant differences for the near-surface relative humidity have been observed between all seasons of the year separately, specially between the summer ans the winter. It is well known that the predominant meteorological situation during the summer over the area of study is associated with mesoscale circulations (Millán et al., 2005). However, during the winter more variability is observed in terms of the dominant atmospheric condition (Estrela et al., 2010). As a consequence, the mentioned differences could also be related to a variance in the RAMS model performance under distinct weather and atmospheric conditions.

Although RAMS has been implemented for a concrete area within the Western Mediterranean Basin, due to its similar climate and physical characteristics, we strongly believe that the results found is this study could be projected as well to other areas in the east coast of the Iberian Peninsula. In addition, the results reproduced in the present paper are analogous to those found in other Mediterranean Regions, using the RAMS model (Pasqui et al., 2004; Federico, 2011), and using other real-time mesoscale models (Bartzokas et al., 2010). Likewise, considering other areas with Mediterranean-type climate regimes, it has been found that atmospheric humidity is the main cause of elevated minimum temperatures in the summer (Gershunov et al., 2009). In contrast, taking into account the temperature field within this season of the year, a cold bias was identified in RAMS simulations over east-central Florida (Case et al., 2002).

Considering the above mentioned points, it is the author's aim to continue the verification of this operational system by testing some improvements found in the model results in diagnostic studies, such as the analysis of the role of the convective parameterization in the precipitation forecasts.

**Acknowledgement**

This work has been funded by the Spanish Ministerio de Educación y Ciencia through the projects CGL2008-04550 (Proyecto NIEVA), CSD2007-00067 CONSOLIDER-INGENIO 2010 (Proyecto GRACCIE) and CGL2007-65774/CLI (Proyecto MAPSAT), and by the Regional Government of Valencia through the contract "Simulación de las olas de calor e invasiones de frío y su regionalización en la Comunitat Valenciana" ("Heat wave and cold invasion simulation and their regionalization at the Valencia Region") and the project PROMETEO/2009/086. The authors wish to thank F. Pastor, J. Miró and M. J. Barberà for their appreciable collaboration as well as to D. Corell for providing the CEAM weather station data and C. Azorín-Molina for his proposals and help while writing this paper. NCEP are acknowledged for providing the GFS meteorological forecasts for RAMS initialization.

**References**

Bartzokas A, Kotroni V, Lagouvardos K, Lolis CJ, Gkikas A, Tsirogianni MI (2010). Weather forecast in north-western Greece: RISKMED warnings and verification of mm5 model. Natural Hazards and Earth System Sciences 10:383-394.

Case JL, Manobianco J, Dianic AV, Wheeler MM, Harms DE, Parks CR (2002). Verification of high-resolution rams forecasts over east-central Florida during the 1999 and 2000 summer months. Weather and Forecasting, 17: 1133-1151.

Chen C, Cotton WR (1983). A one-dimensional simulation of the stratocumulus-capped mixed layer. Boundary-Layer Meteorology, 25: 289-321.

Corell-Custardoy D, Valiente-Pardo JA, Estrela-Navarro MJ, García-Sánchez F, Azorín-Molina C (2010). Red de torres meteorológicas de la Fundación CEAM (CEAM meteorological station network). 2nd Meeting on Meteorology and Climatology of the Western Mediterranean, Valencia, Spain.

Cotton WR, Pielke RAS, Walko RL, Liston GE, Tremback CJ, Jiang H, McAnelly RL, Harrington JY, Nicholls ME, Carrio GG, McFadden JP (2003). RAMS 2001: Current status and future directions. Meteorology and Atmospheric Physics, 82 (1-4): 5-29.

Estrela MJ, Millán MM, Peñarrocha D, Pastor F (2002). De la gota fría al frente de retroceso. Colección Interciencias. UNED, 260 pp. (In Spanish).

Estrela MJ, Valiente JA, Corell D, Millán MM (2008). Fog collection in the western Mediterranean basin (Valencia region, Spain). Atmospheric Research, 87 (3-4): 324-337, doi:10.1016/j.atmosres.2007.11.013.

Estrela MJ, Miró J, Pastor F, Millán M (2010). Frontal Atlantic rainfall component in the Western Mediterranean Basin. Variability and spatial distribution. ESF-MedCLIVAR Workshop on “Hydrological, socioeconomic and ecological impacts of the North Atlantic Oscillation in the Mediterranean region", Zaragoza (Spain), 24-27 May 2010.

Federico S (2011). Verification of surface minimum, mean, and maximum temperature forecasts in Calabria for summer 2008. Natural Hazards and Earth System Sciences 11: 487-500, doi:10.5194/nhess-11-487-2011.

Gershunov A, Cayan D, Iacobellis S (2009). The great 2006 heat wave over California and Nevada: Signal of an increasing trend. Journal of Climate 22: 6181-6203.

Gómez I, Estrela MJ (2010). Design and development of a Java-based graphical user interface to monitor/control a meteorological real-time forecasting system. Computers & Geosciences, 36: 1345-1354, doi:10.1016/j.cageo.2010.05.005.

Gómez I, Pastor F, Estrela MJ (2011). Sensitivity of a mesoscale model to different convective parameterization schemes in a heavy rain event. Natural Hazards and Earth System Sciences, 11: 343-357, doi: 10.5194/nhess-11-343-2011.

Gómez I, Estrela, MJ, Caselles, V (2013). Operational forecasting of daily summer maximum and minimum temperatures in the Valencia Region. Natural Hazards, doi: 10.1007/s11069-013-0861-1.

Gómez-Tejedor JA, Estrela MJ, Millán MM (1999). A mesoscale model application to fire weather winds. International Journal of Wildland Fire, 9: 255-263.

Hernández-Ceballos MA, Adame JA, Bolívar JP, De la Morena BA (2013). A mesoscale simulation of coastal circulation in the Guadalquivir valley (southwestern Iberian Peninsula) using the WRF-ARW model. Atmospheric Research 124: 1-20, doi: 10.1016/j.atmosres.2012.12.002.

Kotroni V, Lagouvardos K, Retalis A (2011). The heat wave of June 2007 in Athens, Greece – Part 2: Modeling study and sensitivity experiments. Atmospheric Research 100: 1–11, doi:10.1016/j.atmosres.2010.12.007.

Martin ML, Santos-Muñoz D, Valero F, Morata A (2010). Evaluation of an ensemble precipitation prediction system over the Western Mediterranean area. Atmospheric Research 98: 163-175, doi: 10.1016/j.atmosres.2010.07.002.

Mazarakis N, Kotroni V, Lagouvardos K, Argiriou A (2009). The sensitivity of numerical forecasts to convective parameterization during the warm period and the use of lightning data as an indicator for convective occurrence. Atmospheric Research 94(4): 704–714, doi:10.1016/j.atmosres.2009.03.002.

Mellor G, Yamada T (1982). Development of a turbulence closure model for geophysical fluid problems. Reviews of Geophysics and Space Physics, 20: 851-875.

Millán M, Estrela MJ, Caselles V (1995). Torrential Precipitations on the Spanish East Coast: The role of the Mediterranean Sea Surface Temperature. Atmospheric Research, 36: 1–16.

Millán MM, Estrela MJ, Miró J (2005). Rainfall components: variability and spatial distribution in a Mediterranean area. Journal of Climate, 18: 2682-2705.

Miró JJ, Estrela MJ, Millán MM (2006). Summer temperature trends in a mediterranean area (Valencia region). International Journal of Climatology, 26: 1051-1073.

Molinari J. 1985. A general form of Kuo's cumulus parameterization. Monthly Weather Review, 113: 1411-1416.

Palau JL, Pérez-Landa G, Diéguez JJ, Monter C, Millán MM (2005). The importance of meteorological scales to forecast air pollution scenarios on coastal complex terrain. Atmospheric Chemistry and Physics 5:2771-2785.

Papanastasiou DK, Melas D, Lissaridis I (2010). Study of wind field under sea breeze conditions; an application of WRF model. Atmospheric Research 98: 102-117, doi: 10.1016/j.atmosres.2010.06.005.

Pasqui M, Gioli B, Gozzini B, Miglietta F (2004). Atmospheric Regional Reanalysis simulations, based on RAMS model, as input for crop modelling. 26th Conference on Agricultural and Forest Meteorology.

Pérez-Landa G, Ciais P, Sanz MJ, Gioli B, Miglietta F, Palau JL, Gangoiti G, Millán M (2007). Mesoscale circulations over complex terrain in the Valencia coastal region, Spain. Part 1: Simulation of diurnal circulation regimes. Atmospheric Chemistry and Physics 7:1835-1849.

Pielke Sr. RA (2002). Mesoscale meteorological modeling. 2nd Edition. Academic Press, San Diego, CA, 676 pp.

Rossa A, Nurmi P, Ebert E (2008). Overview of methods for the verification of quantitative precipitation forecasts. In: Michaelides, S (Ed.). Precipitation: Advances in Measurement, Estimation and Prediction. Springer, pp. 419-452.

Walko RL, Cotton WR, Meyers MP, Harrington JY (1995). New RAMS cloud microphysics parameterization. Part I: The single-moment scheme. Atmospheric Research, 38: 29-62.

Walko RL, Band LE, Baron J, Kittel TGF, Lammers R, Lee TJ, Ojima D, Pielke RA, Taylor C, Tague C, Tremback CJ, Vidale PL (2000). Coupled atmospheric-biophysics-hydrology models for environmental modeling. Journal of Applied Meteorology, 39: 931-944.

## Figure captions

Fig. 1. RAMS model domain configuration and orography (m) of the Valencia Region (Domain 3) with the location of the representative coastal and inland CEAM weather stations.

Fig. 2. Measured (continuous line) and simulated (discontinuous line) near-surface temperature (ºC) and relative humidity (%) time series, for the different seasons of the year. Coastal stations: spring (a), summer (c), fall (e) and winter (g). Inland stations: spring (b), summer (d), fall (f) and winter (h).

Fig. 3. Scatterplot of the simulated near-surface temperature (ºC) versus the measured temperature (ºC) at 05 and 13 UTC, for the different seasons of the year. Coastal stations: spring (a), summer (c), fall (e) and winter (g). Inland stations: spring (b), summer (d), fall (f) and winter (h).

Fig 4. Same as Fig. 3, but for the near-surface relative humidity (%).

Fig. 5. Same as Fig. 2, but for the near-surface wind speed (m/s) and direction (deg).

Fig. 6. Same as Fig. 3, but for the near-surface wind speed (m/s).

Fig. 7. Scatterplot of 24-h accumulated precipitation for the second day of simulation: spring (a), summer (b), fall (c) and winter (d).

Fig. 8. Scatterplot of 6-h intervals accumulated precipitation for the second day of simulation. Spring: 00:00-06:00 UTC (a), 06:00-12:00 UTC (b), 12:00-18:00 UTC (c) and 18:00-24:00 UTC (d). Summer: 00:00-06:00 UTC (e), 06:00-12:00 UTC (f), 12:00-18:00 UTC (g) and 18:00-24:00 UTC (h).

Fig. 9. Same as Fig. 8, but for the fall: 00:00-06:00 UTC (a), 06:00-12:00 UTC (b), 12:00-18:00 UTC (c) and 18:00-24:00 UTC (d), and the winter: 00:00-06:00 UTC (e), 06:00-12:00 UTC (f), 12:00-18:00 UTC (g) and 18:00-24:00 UTC (h).

**Tables**

Table 1. Rams model settings for the three simulation grids: number of grid points in the x, y and z directions (nx, ny and nz), horizontal grid spacing (dx) and timestep (t).

| Grid | nx | ny | nz | dx (m) | t (s) |
|---|---|---|---|---|---|
| 1 | 83 | 58 | 24 | 48000 | 60 |
| 2 | 146 | 94 | 24 | 12000 | 30 |
| 3 | 78 | 126 | 24 | 3000 | 10 |

Table 2. Model skill against surface observations for the first day of simulation and the different seasons of the year. Index of agreement, Bias and RMSE are included for the near-surface temperature (ºC) and relative humidity (%). The ”Night” value is that obtained at 05:00 UTC while the “Day” value corresponds to the one calculated at 13:00 UTC. “All” value is the one taking into account all daily data.

| | | Temperature | | | Relative Humidity | | |
|---|---|---|---|---|---|---|---|
| Station | Period | IoA | Bias | RMSE | IoA | Bias | RMSE |
| | | Spring | | | | | |
| All | All | 0.9 | 1.0 | 4 | 0.8 | -8 | 21 |
| | Day | 0.9 | 0.006 | 3 | 0.8 | -3 | 18 |
| | Night | 0.8 | 1.6 | 4 | 0.6 | -11 | 23 |
| Coastal | All | 0.9 | 0.4 | 3 | 0.8 | -6 | 20 |
| | Day | 0.9 | -0.4 | 3 | 0.8 | -3 | 18 |
| | Night | 0.8 | 0.6 | 3 | 0.7 | -8 | 22 |
| Inland | All | 0.9 | 1.3 | 4 | 0.8 | -8 | 22 |
| | Day | 0.9 | 0.2 | 3 | 0.8 | -2 | 17 |
| | Night | 0.8 | 2 | 4 | 0.5 | -13 | 24 |
| | | Summer | | | | | |
| All | All | 0.9 | 1.4 | 3 | 0.7 | -15 | 23 |
| | Day | 0.9 | 0.17 | 3 | 0.7 | -8 | 16 |
| | Night | 0.8 | 1.9 | 4 | 0.6 | -17 | 25 |
| Coastal | All | 0.9 | 0.4 | 3 | 0.7 | -12 | 20 |
| | Day | 0.9 | -0.4 | 2 | 0.7 | -9 | 16 |
| | Night | 0.8 | 0.7 | 2 | 0.6 | -13 | 22 |
| Inland | All | 0.9 | 2 | 4 | 0.7 | -16 | 24 |
| | Day | 0.9 | 0.4 | 3 | 0.7 | -8 | 16 |
| | Night | 0.7 | 3 | 4 | 0.5 | -20 | 30 |
| | | Fall | | | | | |
| All | All | 0.9 | 0.2 | 3 | 0.8 | -5 | 19 |
| | Day | 0.9 | -1.1 | 3 | 0.8 | -0.7 | 16 |
| | Night | 0.9 | 1.0 | 4 | 0.6 | -7 | 21 |
| Coastal | All | 0.9 | -0.5 | 3 | 0.8 | -3 | 18 |
| | Day | 0.9 | -1.6 | 3 | 0.8 | -1.3 | 15 |
| | Night | 0.9 | -0.04 | 3 | 0.7 | -4 | 19 |
| Inland | All | 0.9 | 0.6 | 3 | 0.8 | -6 | 20 |
| | Day | 0.9 | -0.9 | 3 | 0.8 | -0.4 | 16 |
| | Night | 0.9 | 1.5 | 4 | 0.6 | -9 | 21 |
| | | Winter | | | | | |
| All | All | 0.8 | 0.4 | 4 | 0.7 | -4 | 19 |
| | Day | 0.9 | -0.9 | 3 | 0.8 | -0.2 | 16 |
| | Night | 0.8 | 0.8 | 4 | 0.6 | -6 | 20 |
| Coastal | All | 0.8 | -0.3 | 4 | 0.8 | -2 | 18 |
| | Day | 0.8 | -1.4 | 4 | 0.8 | 0.7 | 17 |
| | Night | 0.8 | -0.16 | 3 | 0.7 | -3 | 18 |
| Inland | All | 0.8 | 0.7 | 4 | 0.7 | -5 | 20 |
| | Day | 0.9 | -0.7 | 3 | 0.8 | -0.7 | 16 |
| | Night | 0.7 | 1.3 | 4 | 0.6 | -7 | 21 |

Table 3. Model skill against surface observations for the first day of simulation and the different seasons of the year. Index of agreement, Bias and RMSE are included for the near-surface wind speed (m/s). The VWD-RMSE statistic is included for the wind direction (m/s). The “Night“ value is that obtained at 05:00 UTC while the ”Day“ values corresponds to the one computed at 13:00 UTC. ”All“ value is the one taking into account all daily data.

| | | | Wind Speed | | VWD |
|---|---|---|---|---|---|
| | | | Spring | | |
| Station | Period | IoA | Bias | RMSE | RMSE |
| All | All | 0.7 | 0.9 | 2 | 4 |
| | Day | 0.5 | 1.5 | 3 | 5 |
| | Night | 0.7 | 1.0 | 2 | 3 |
| Coastal | All | 0.7 | 1.1 | 2 | 4 |
| | Day | 0.5 | 1.9 | 3 | 5 |
| | Night | 0.6 | 1.2 | 2 | 3 |
| Inland | All | 0.7 | 0.8 | 2 | 4 |
| | Day | 0.5 | 1.3 | 3 | 5 |
| | Night | 0.7 | 0.9 | 2 | 3 |
| | | | Summer | | |
| Station | Period | IoA | Bias | RMSE | RMSE |
| All | All | 0.7 | 1.5 | 2 | 4 |
| | Day | 0.4 | 3 | 3 | 5 |
| | Night | 0.5 | 1.1 | 1.9 | 3 |
| Coastal | All | 0.7 | 1.5 | 2 | 4 |
| | Day | 0.4 | 3 | 3 | 5 |
| | Night | 0.5 | 0.9 | 1.8 | 3 |
| Inland | All | 0.7 | 1.5 | 2 | 4 |
| | Day | 0.4 | 3 | 3 | 5 |
| | Night | 0.5 | 1.2 | 2 | 3 |
| | | | Fall | | |
| Station | Period | IoA | Bias | RMSE | RMSE |
| All | All | 0.7 | 1.0 | 2 | 4 |
| | Day | 0.6 | 1.5 | 3 | 4 |
| | Night | 0.7 | 1.1 | 2 | 3 |
| Coastal | All | 0.7 | 1.2 | 2 | 3 |
| | Day | 0.5 | 2 | 3 | 4 |
| | Night | 0.6 | 1.1 | 2 | 3 |
| Inland | All | 0.7 | 0.9 | 2 | 4 |
| | Day | 0.6 | 1.3 | 3 | 4 |
| | Night | 0.7 | 1.1 | 2 | 3 |
| | | | Winter | | |
| Station | Period | IoA | Bias | RMSE | RMSE |
| All | All | 0.7 | 0.5 | 2 | 4 |
| | Day | 0.7 | 0.17 | 2 | 4 |
| | Night | 0.7 | 0.8 | 2 | 4 |
| Coastal | All | 0.7 | 0.9 | 2 | 4 |
| | Day | 0.7 | 0.5 | 2 | 4 |
| | Night | 0.6 | 1.2 | 3 | 4 |
| Inland | All | 0.7 | -0.3 | 2 | 4 |
| | Day | 0.7 | 0.02 | 2 | 4 |
| | Night | 0.7 | 0.6 | 2 | 4 |

Table 4. Categorical statistics for 24-h accumulated precipitation for all seasons of the year and the second day of simulation.

| Categorical Scores | Daily (24-h) | | | | | | | |
|---|---|---|---|---|---|---|---|---|
| | Spring | | | | Summer | | | |
| | ≥ 2mm | ≥ 8mm | ≥ 15mm | ≥ 30mm | ≥ 2mm | ≥ 8mm | ≥ 15mm | ≥ 30mm |
| AC | 0.8 | 0.9 | 0.9 | 1.0 | 0.9 | 1.0 | 1.0 | 1.0 |
| Bias | 1.5 | 1.9 | 2.4 | 4 | 1.0 | 1.2 | 2 | 3 |
| POD | 0.6 | 0.4 | 0.2 | 0.1 | 0.2 | 0.15 | 0.05 | 0.07 |
| FAR | 0.6 | 0.8 | 0.9 | 1.0 | 0.8 | 0.9 | 1.0 | 1.0 |
| CSI | 0.3 | 0.18 | 0.07 | 0.03 | 0.13 | 0.08 | 0.016 | 0.019 |
| HSS | 0.4 | 0.3 | 0.11 | 0.04 | 0.2 | 0.12 | 0.02 | 0.03 |
| | Fall | | | | Winter | | | |
| AC | 0.8 | 0.9 | 0.9 | 1.0 | 0.8 | 0.9 | 1.0 | 1.0 |
| Bias | 1.2 | 1.1 | 1.1 | 1.1 | 1.4 | 1.7 | 1.7 | 1.5 |
| POD | 0.5 | 0.3 | 0.2 | 0.10 | 0.6 | 0.4 | 0.3 | 0.2 |
| FAR | 0.6 | 0.7 | 0.8 | 0.9 | 0.6 | 0.7 | 0.8 | 0.9 |
| CSI | 0.3 | 0.18 | 0.11 | 0.05 | 0.3 | 0.2 | 0.11 | 0.09 |
| HSS | 0.4 | 0.3 | 0.17 | 0.08 | 0.4 | 0.3 | 0.18 | 0.16 |

Table 5. Categorical statistics for the first 6-hour interval (00:00-06:00 UTC) accumulated precipitation for all seasons of the year and the second day of simulation.

| Categorical Scores | First 6-h interval (00:00-06:00 UTC) accumulated precipitation | | | | | |
|---|---|---|---|---|---|---|
| | Spring | | | Summer | | |
| | ≥ 2mm | ≥ 8mm | ≥ 15mm | ≥ 2mm | ≥ 8mm | ≥ 15mm |
| AC | 1.0 | 1.0 | 1.0 | 1.0 | 1.0 | - |
| Bias | 1.4 | 1.8 | 1.4 | 0.5 | 0.12 | - |
| POD | 0.4 | 0.18 | 0 | 0 | 0 | - |
| FAR | 0.7 | 0.9 | 1.0 | 1.0 | 1.0 | - |
| CSI | 0.2 | 0.07 | 0.0 | 0 | 0 | - |
| HSS | 0.3 | 0.13 | -0.0014 | 0.006 | -0.0006 | - |
| | Fall | | | Winter | | |
| AC | 0.9 | 1.0 | 1.0 | 0.9 | 1.0 | 1.0 |
| Bias | 1.1 | 0.9 | 0.5 | 1.5 | 2 | 3.6 |
| POD | 0.3 | 0.02 | 0 | 0.4 | 0.18 | 0.2 |
| FAR | 0.8 | 1.0 | 1.0 | 0.8 | 0.9 | 0.9 |
| CSI | 0.14 | 0.011 | 0 | 0.2 | 0.06 | 0.05 |
| HSS | 0.2 | 0.008 | -0.006 | 0.3 | 0.11 | 0.09 |

Table 6. Categorical statistics for the second 6-hour interval (06:00-12:00 UTC) accumulated precipitation for all seasons of the year and the second day of simulation.

| Categorical Scores | Second 6-h interval (06:00-12:00 UTC) accumulated precipitation | | | | | |
|---|---|---|---|---|---|---|
| | Spring | | | Summer | | |
| | ≥ 2mm | ≥ 8mm | ≥ 15mm | ≥ 2mm | ≥ 8mm | ≥ 15mm |
| AC | 0.9 | 1.0 | 1.0 | 1.0 | 1.0 | 1.0 |
| Bias | 1.6 | 1.4 | 3 | 0.6 | 0.8 | 1.6 |
| POD | 0.3 | 0.03 | 0 | 0.1 | 0 | 0 |
| FAR | 0.8 | 1.0 | 1.0 | 0.8 | 1.0 | 1.0 |
| CSI | 0.13 | 0.014 | 0 | 0.07 | 0 | 0 |
| HSS | 0.2 | 0.02 | -0.002 | 0.12 | -0.003 | -0.0011 |
| | Fall | | | Winter | | |
| AC | 0.9 | 1.0 | 1.0 | 0.9 | 1.0 | 1.0 |
| Bias | 1.1 | 1.0 | 0.6 | 1.6 | 1.4 | 2 |
| POD | 0.4 | 0.17 | 0.13 | 0.3 | 0.2 | 0.17 |
| FAR | 0.7 | 0.8 | 0.8 | 0.8 | 0.8 | 0.9 |
| CSI | 0.2 | 0.09 | 0.09 | 0.15 | 0.11 | 0.06 |
| HSS | 0.3 | 0.16 | 0.15 | 0.2 | 0.2 | 0.10 |

Table 7. Categorical statistics for the third 6-hour interval (12:00-18:00 UTC) accumulated precipitation for all seasons of the year and the second day of simulation.

| Categorical Scores | Third 6-h interval (12:00-18:00 UTC) accumulated precipitation | | | | | |
|---|---|---|---|---|---|---|
| | Spring | | | Summer | | |
| | ≥ 2mm | ≥ 8mm | ≥ 15mm | ≥ 2mm | ≥ 8mm | ≥ 15mm |
| AC | 0.9 | 1.0 | 1.0 | 0.9 | 1.0 | 1.0 |
| Bias | 1.8 | 2 | 3 | 1.4 | 2 | 4 |
| POD | 0.4 | 0.18 | 0 | 0.2 | 0.18 | 0.14 |
| FAR | 0.8 | 0.9 | 1.0 | 0.8 | 0.9 | 1.0 |
| CSI | 0.17 | 0.06 | 0 | 0.10 | 0.06 | 0.03 |
| HSS | 0.2 | 0.10 | -0.009 | 0.16 | 0.10 | 0.05 |
| | Fall | | | Winter | | |
| AC | 0.9 | 1.0 | 1.0 | 0.9 | 1.0 | 1.0 |
| Bias | 1.3 | 1.2 | 1.5 | 1.4 | 1.6 | 1.5 |
| POD | 0.3 | 0.16 | 0.08 | 0.3 | 0.06 | 0 |
| FAR | 0.8 | 0.9 | 0.9 | 0.8 | 1.0 | 1.0 |
| CSI | 0.13 | 0.08 | 0.03 | 0.14 | 0.02 | 0 |
| HSS | 0.18 | 0.12 | 0.05 | 0.2 | 0.04 | -0.004 |

Table 8. Categorical statistics for the fourth 6-hour interval (18:00-24:00 UTC) accumulated precipitation for all seasons of the year and the second day of simulation.

| Categorical Scores | Fourth 6-h interval (18:00-24:00 UTC) accumulated precipitation | | | | | |
|---|---|---|---|---|---|---|
| | Spring | | | Summer | | |
| | ≥ 2mm | ≥ 8mm | ≥ 15mm | ≥ 2mm | ≥ 8mm | ≥ 15mm |
| AC | 0.9 | 1.0 | 1.0 | 1.0 | 1.0 | 1.0 |
| Bias | 1.8 | 1.6 | 3 | 0.8 | 1.0 | 2 |
| POD | 0.3 | 0.07 | 0 | 0.08 | 0 | 0 |
| FAR | 0.8 | 1.0 | 1.0 | 0.9 | 1.0 | 1.0 |
| CSI | 0.13 | 0.03 | 0 | 0.05 | 0 | 0 |
| HSS | 0.17 | 0.04 | -0.004 | 0.07 | -0.005 | -0.002 |
| | Fall | | | Winter | | |
| AC | 0.9 | 1.0 | 1.0 | 0.9 | 1.0 | 1.0 |
| Bias | 1.5 | 1.1 | 0.9 | 1.4 | 0.8 | 1.0 |
| POD | 0.15 | 0 | 0 | 0.4 | 0.11 | 0.11 |
| FAR | 0.9 | 1.0 | 1.0 | 0.7 | 0.9 | 0.9 |
| CSI | 0.07 | 0 | 0 | 0.2 | 0.06 | 0.06 |
| HSS | 0.08 | -0.017 | -0.008 | 0.3 | 0.11 | 0.11 |

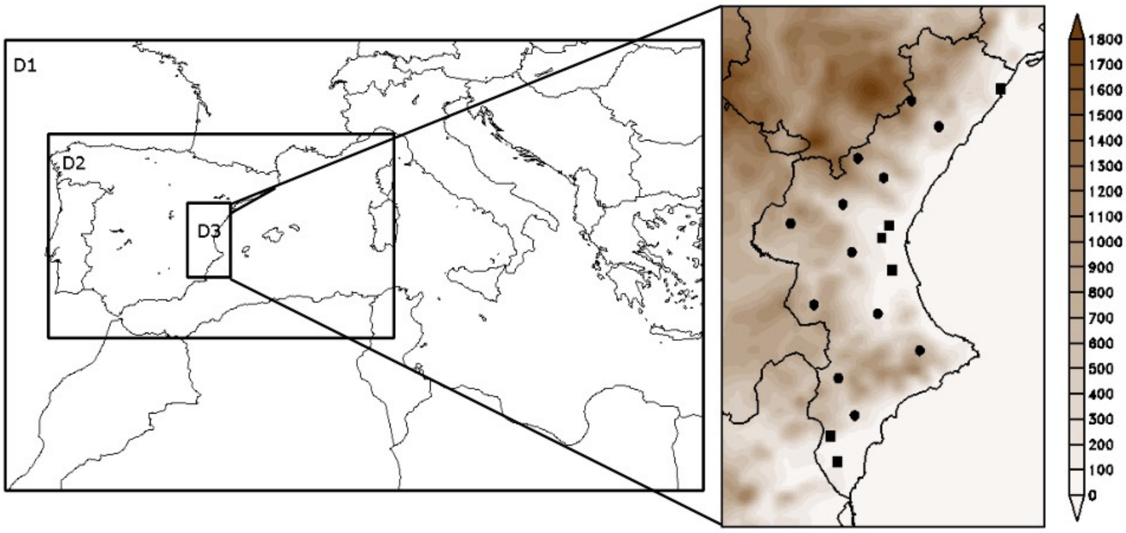
D1
D2
D3
1800
1700
1600
1500
1400
1300
1200
1100
1000
900
800
700
600
500
400
300
200
100
0

Figure 1

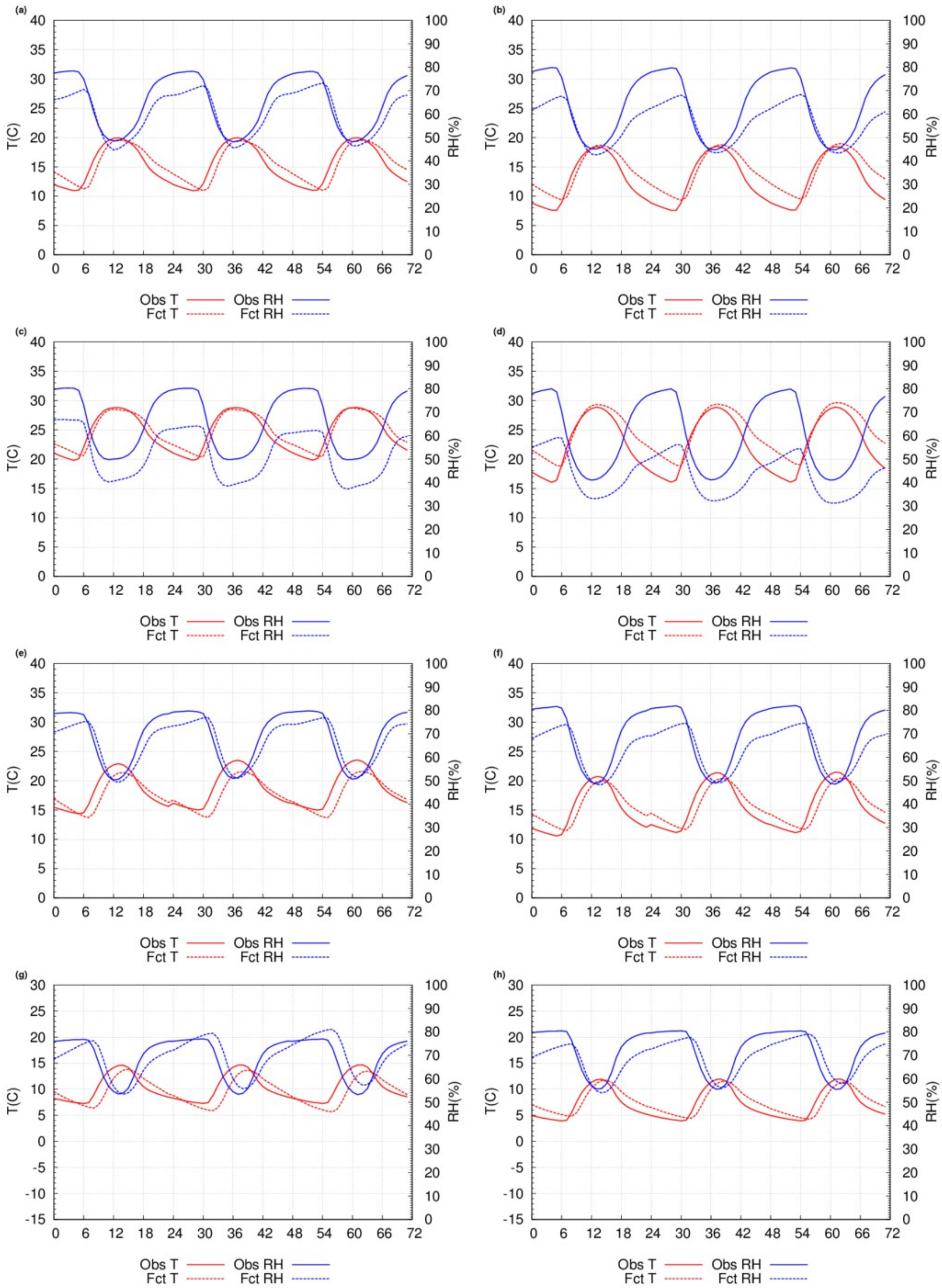


Figure 2

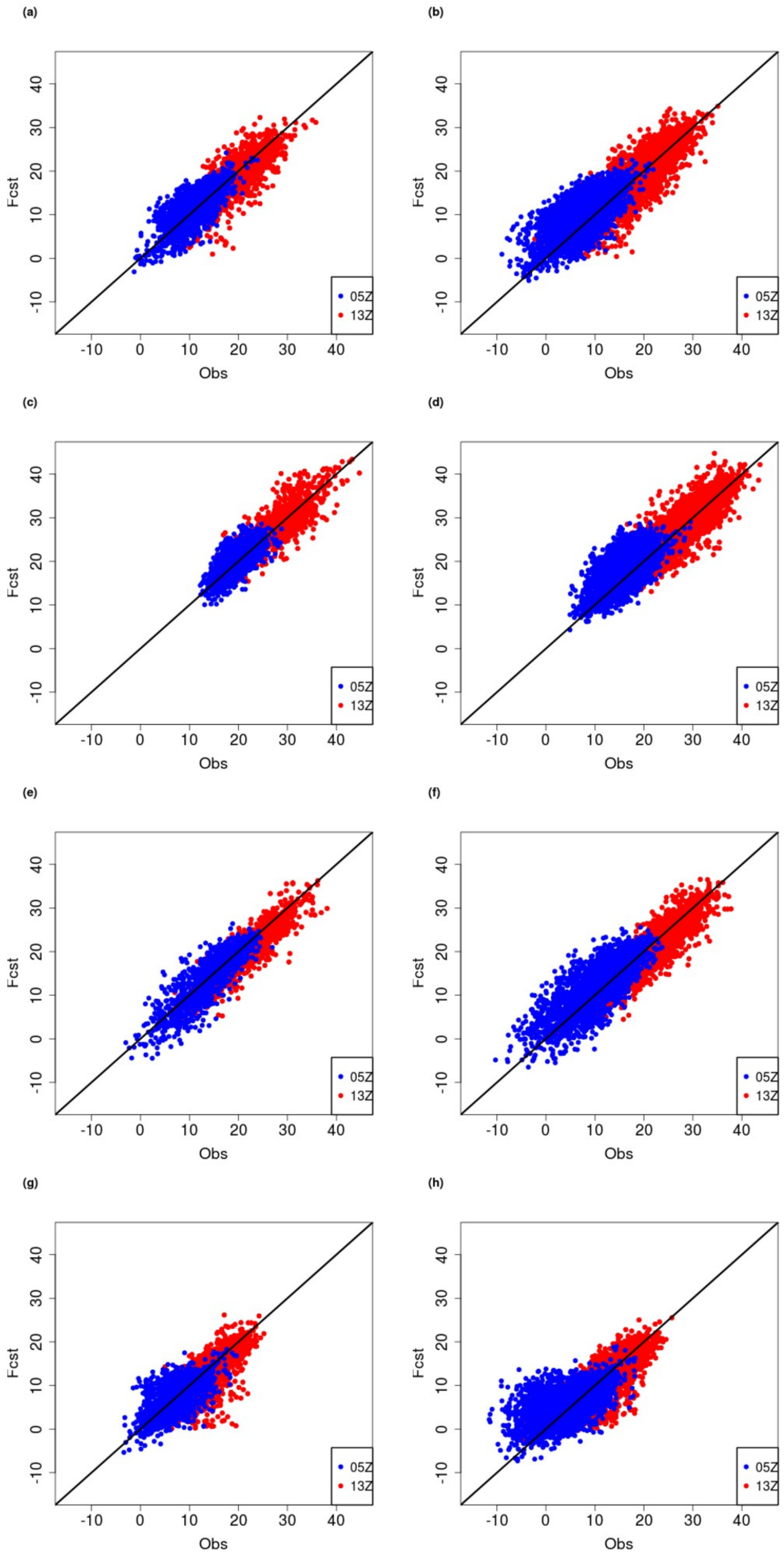


Figure 3

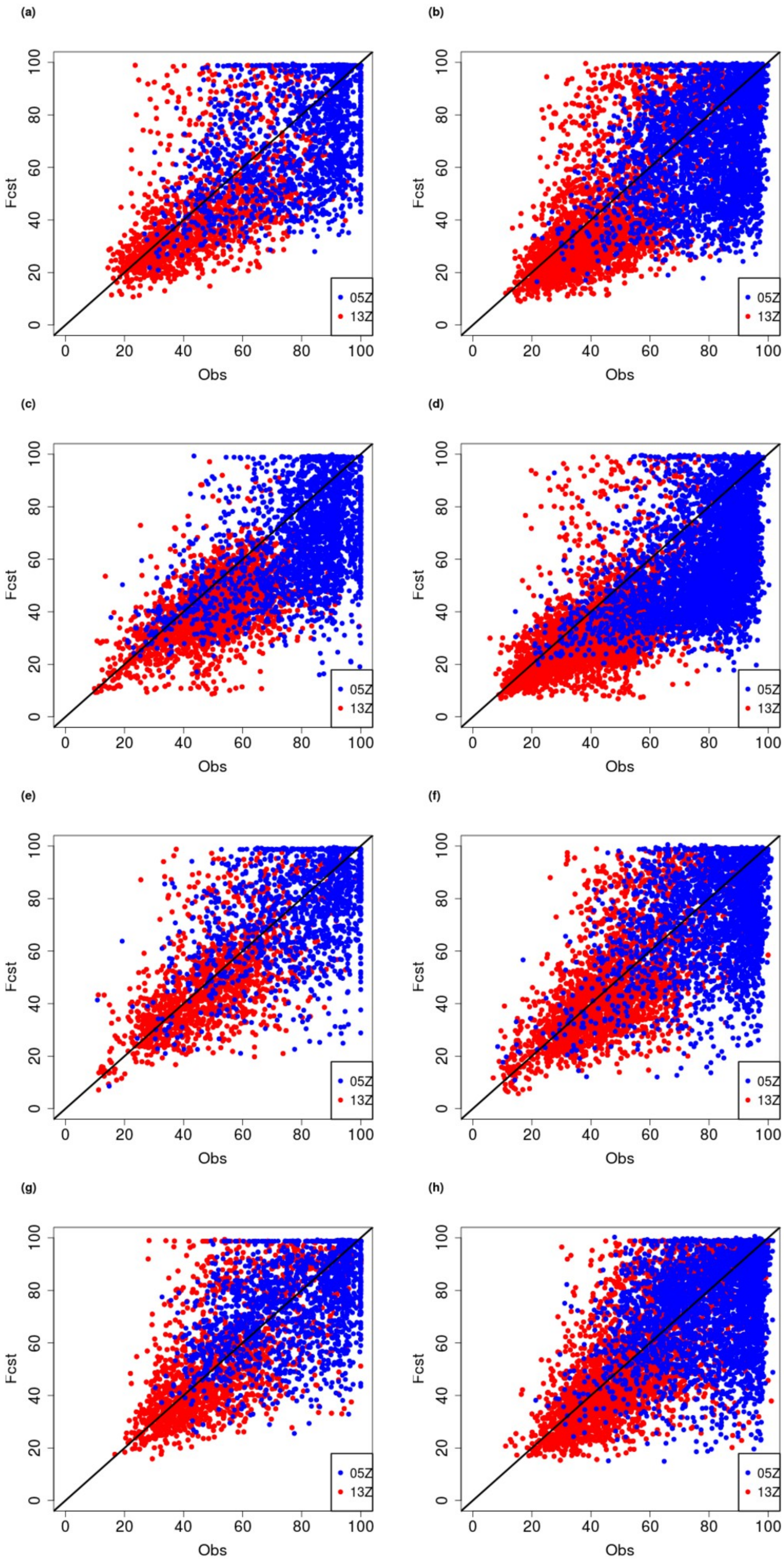


946 Figure 4

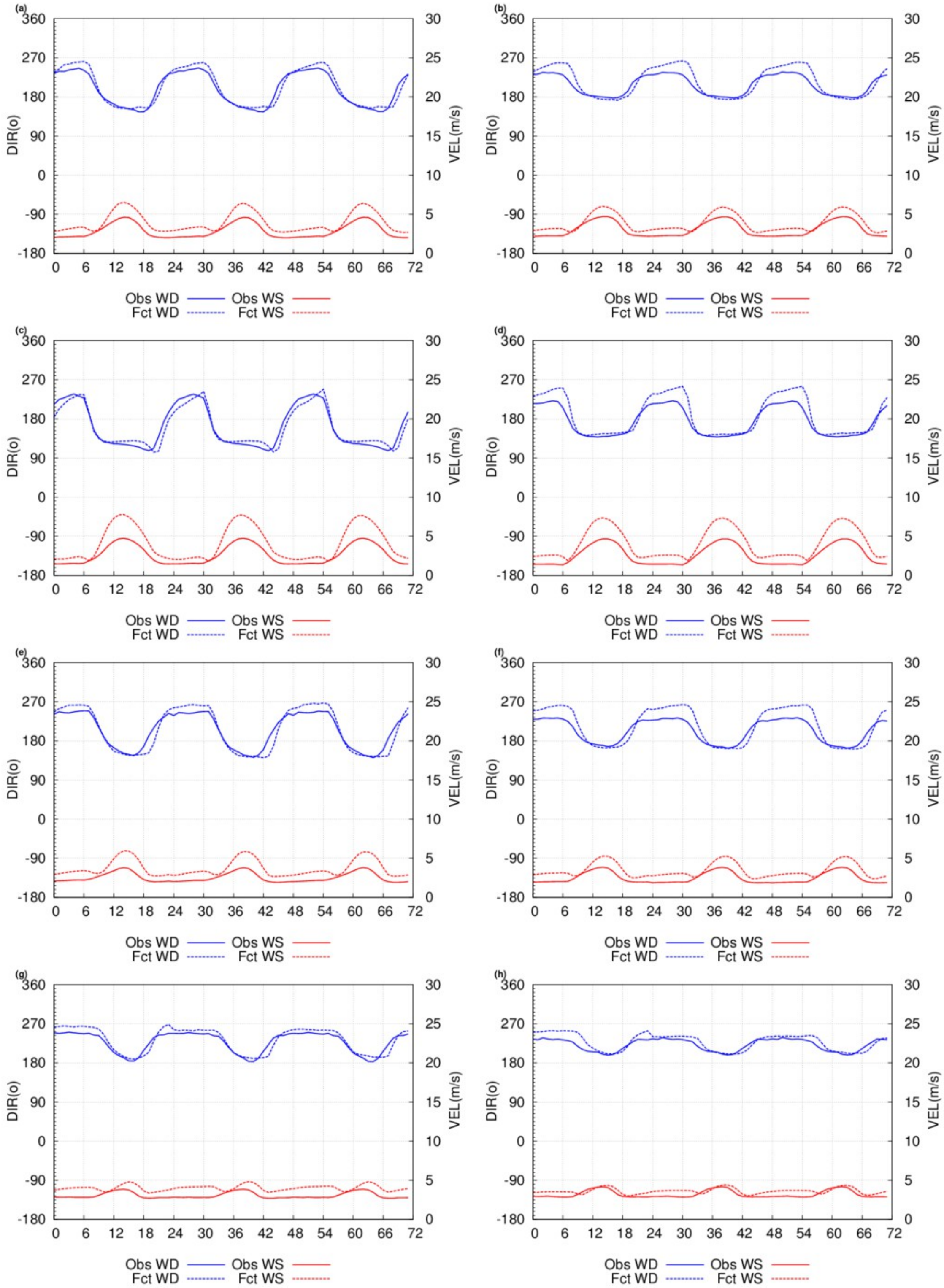


Figure 5

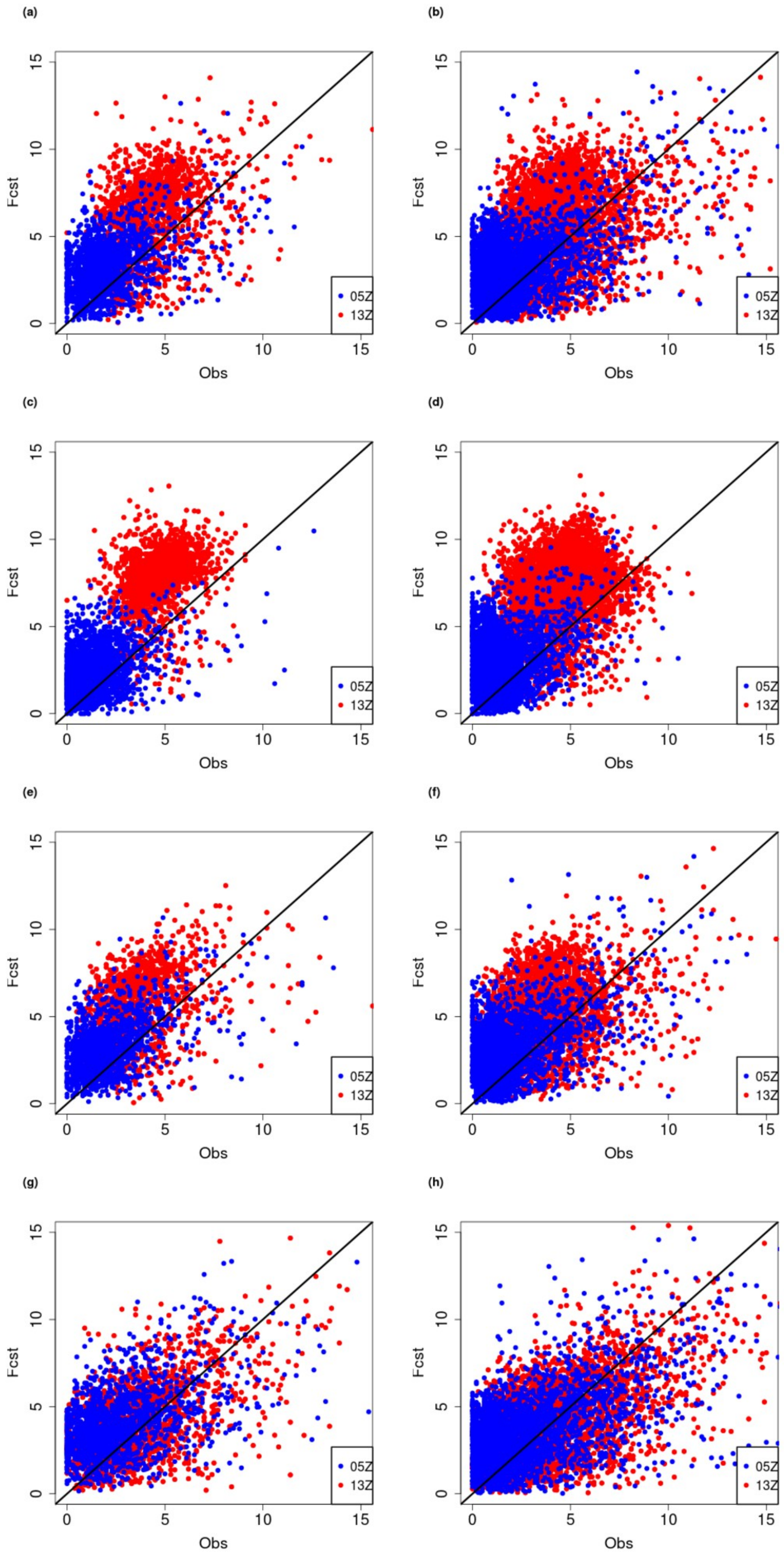


951 Figure 6

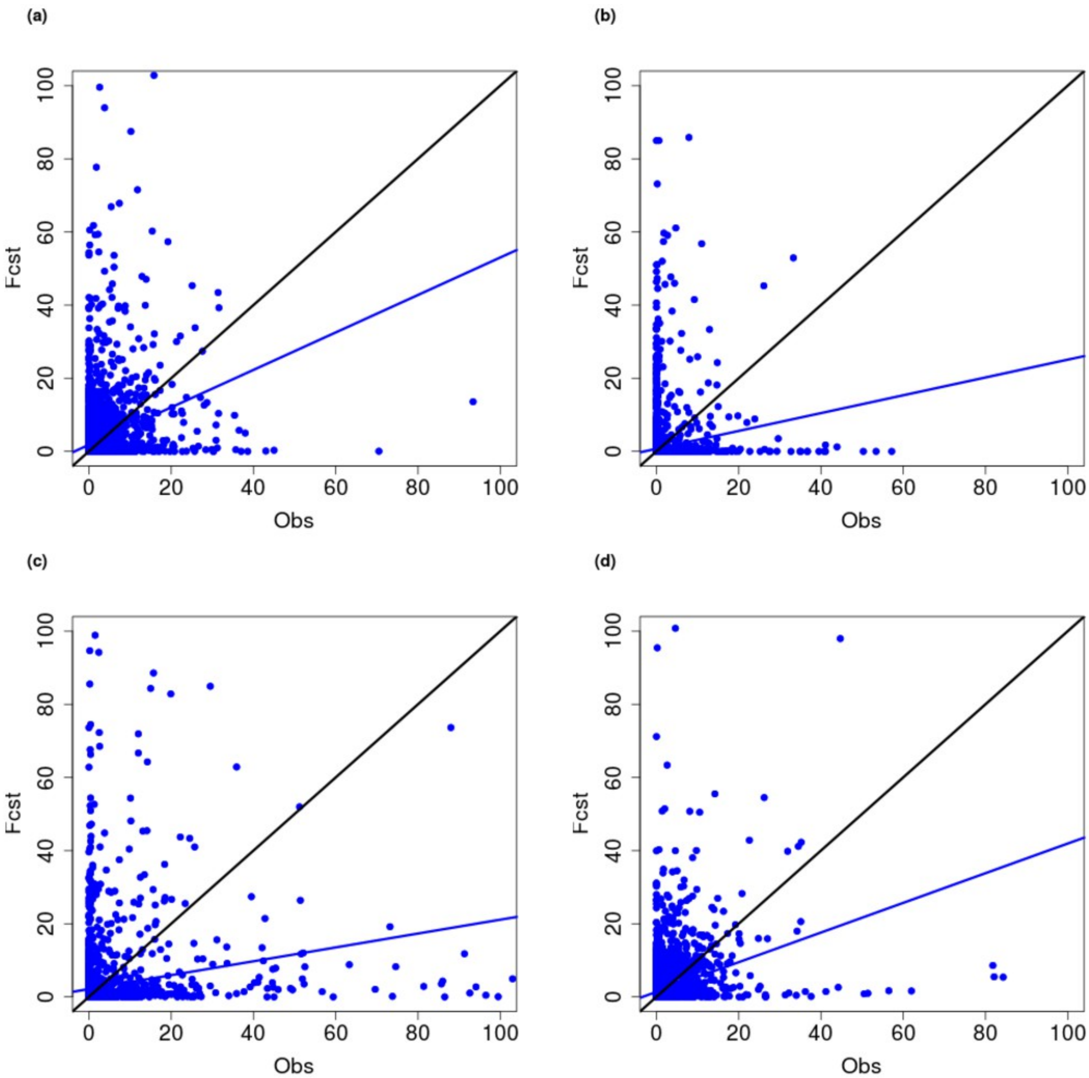


953 Figure 7

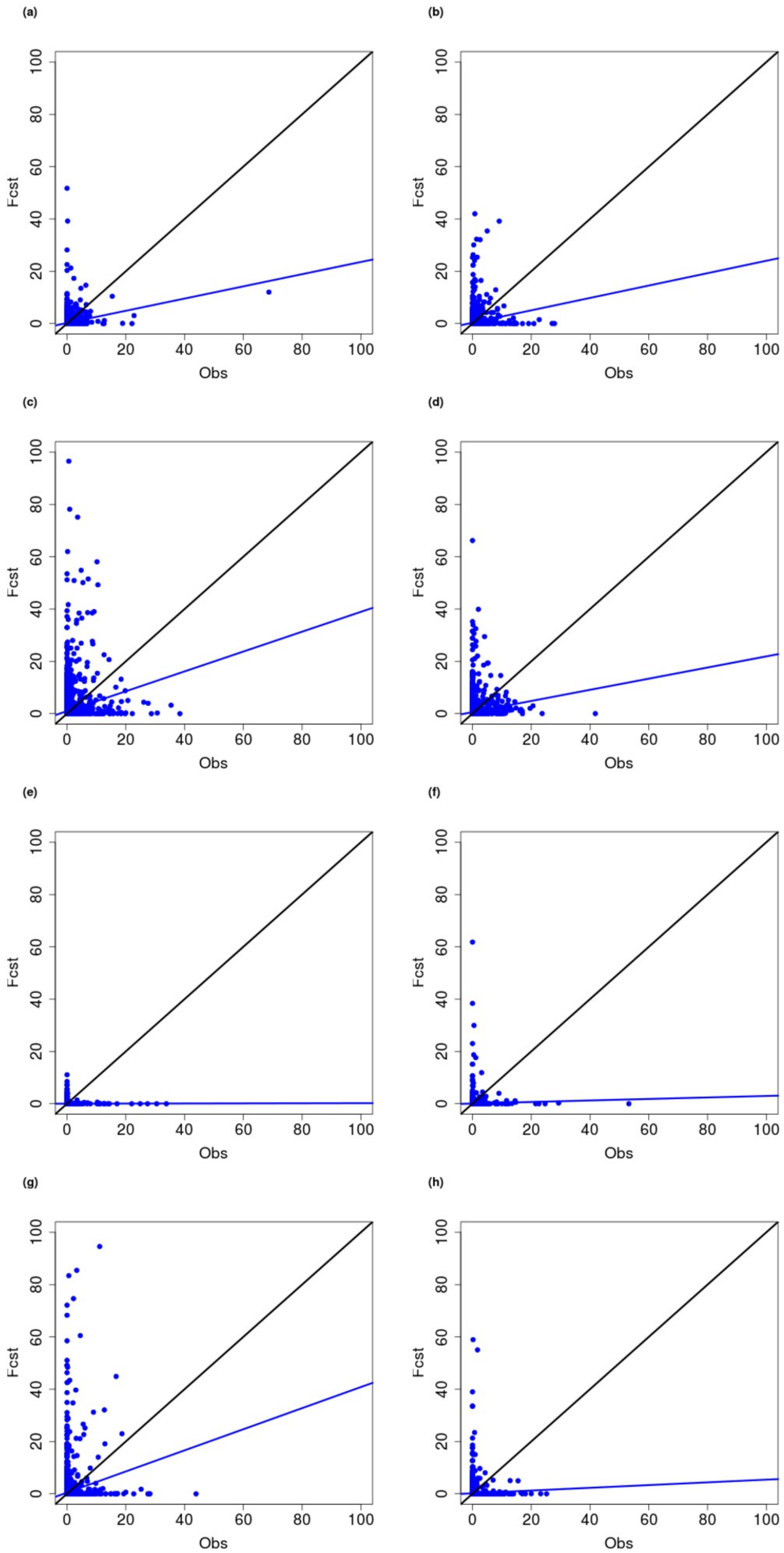


955 Figure 8

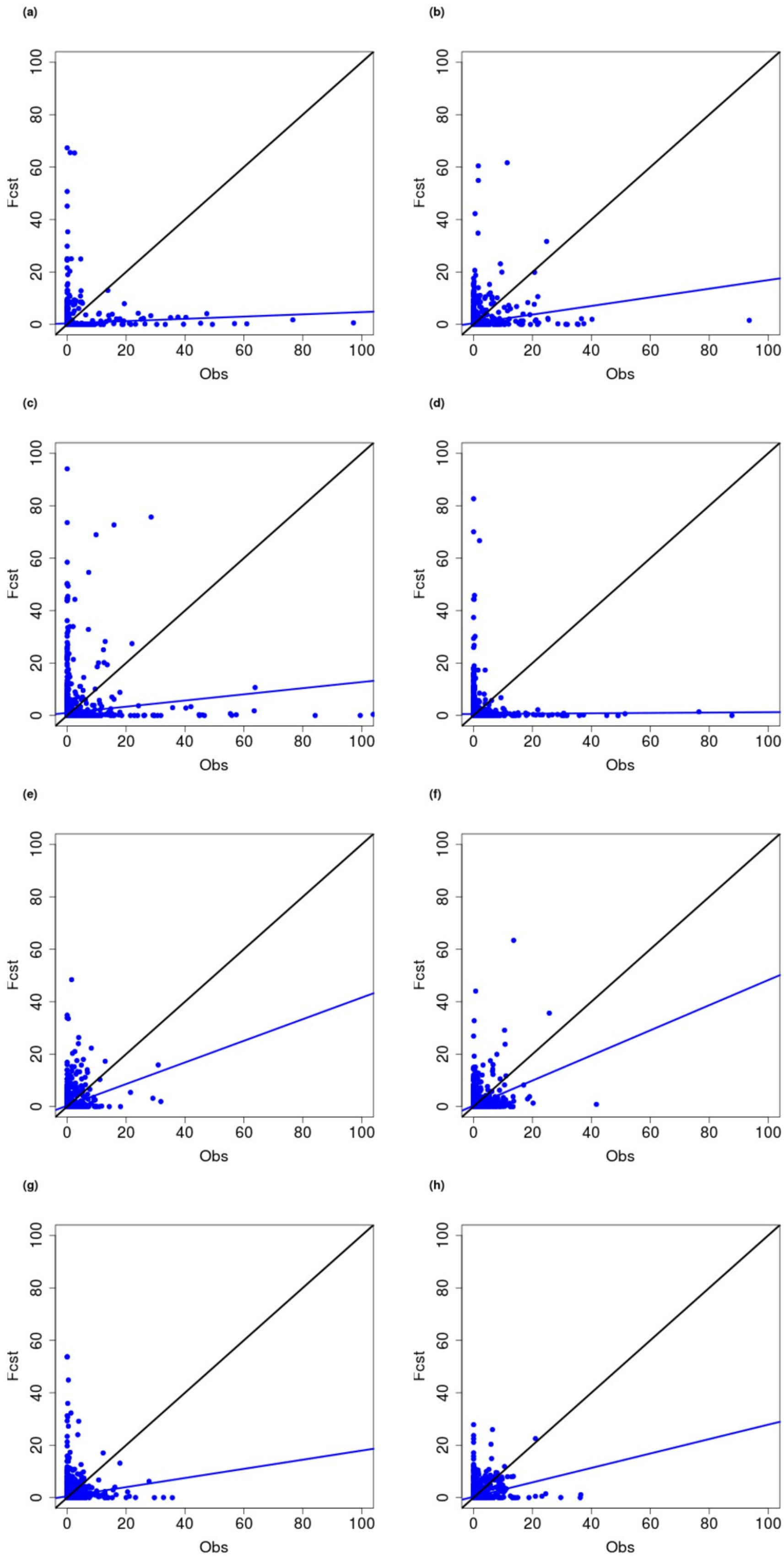


Figure 9